Journal of Alloys and Compounds 509 (2011) 6056–6060

Contents lists available at ScienceDirect

Journal of Alloys and Compounds

journal homepage: www.elsevier.com/locate/jallcom

Multiferroic behavior in glass–crystal nanocomposites containing Te_2NiMnO_6

R.P. Maiti [a], S. Dutta [b], S. Basu [c], M.K. Mitra [a], Dipankar Chakravorty [d,*]

[a] Department of Metallurgical & Material Engineering, Jadavpur University, Kolkata 700 032, India
[b] Rammonhan College, 102/1 Raja Rammohon Roy Sarani, Kolkata 700 009, India
[c] National Institute of Technology, Durgapur 713209, West Bengal, India
[d] DST Unit on Nano Science, Indian Association for the Cultivation of Science, Kolkata 700 032, India

ARTICLE INFO

Article history:
Received 9 October 2010
Received in revised form 28 February 2011
Accepted 2 March 2011
Available online 10 March 2011

Keywords:
Te_2NiMnO_6
Nanocomposite
Double perovskite
Multiferroic

ABSTRACT

Nanocomposites containing nanocrystals of Te_2NiMnO_6 were synthesized by suitable heat treatment of a glass with composition 2 TeO_2·NiO·MnO (molar ratio). The crystallites had dimensions in the range 17–41 nm. X-ray diffraction data of the specimens were analyzed by using a TREOR computer programme. Lattice parameters extracted by this method indicated that the crystal symmetry was monoclinic. The nanocomposites exhibited weak ferromagnetism in the temperature range 2–300 K. They also showed ferroelectric hysteresis at room temperature with a remanent polarization of 0.015 μC/cm^2. The specimens showed a magnetodielectric (MD) behavior with dielectric constant increasing as a function of applied magnetic field. The MD parameter obtained in the present system was 0.55%.

1. Introduction

Multiferroics exhibiting both ferroelectric and ferromagnetic order has been an active area of research during the last couple of years. Multiferroic $YbMnO_3$ ceramics showed aging phenomenon which arose due to the time-dependent formation of positively charged oxygen vacancies and negatively charged Mn defects [1]. A sol–gel route using inorganic salts to synthesize multiferroic lead iron tungstate, $Pb(Fe_{2/3}W_{1/3})O_3$ has been reported which leads to a high purity perovskite phase at a much lower temperature of treatment than was possible earlier [2]. Also formation of the detrimental pyrochlore phase ($Pb_2FeWO_{6.5}$) could be averted by this method. $PbTiO_3/NiFe_2O_4$ multiferroic composite thin films were prepared by a sol–gel in situ method which gave good multifunctional properties [3]. $BiFeO_3$–$BaTiO_3$ multiferroic ceramics have been made by a solid state reaction method which exhibit better dielectric and magnetization properties than reported earlier [4]. Multiferroic properties of the ternary system $BiFeO_3$–$BiMgTiO_3$–$PbTiO_3$ prepared by high temperature solid state reaction route were investigated [5]. These materials exhibited high dielectric constant with a reduced electrical leakage current. Electron paramagnetic resonance spectra were used to study the ferro-paraelectric and antiferro-paramagnetic transitions in the magnetoelectric material $Pb(Fe_{0.5}Ta_{0.5})O_3$ [6]. Clear evidence of the presence of electric and magnetic orders was obtained by this technique. Lanthanum doped $BiFeO_3$ synthesized by sol–gel method followed by rapid sintering has been shown to contain no impurity phase which otherwise has a deleterious effect on its multiferroic behavior [7]. Doping of $BiFeO_3$ by other ions also has been reported with improvement in the dielectric/magnetic properties [8–14]. Newer synthesis techniques have been reported for making $BiFeO_3$ powders [15–18] and thin films of $BiFeO_3$ [19–21]. Thin films of a non-perovskite structured compound CdTe with Mn doping have been grown by pulsed laser deposition technique. The films have been reported to show multiferroic behavior [22]. Highly oriented $Pb(Zr_{0.53}Ti_{0.47})_{0.60}(Fe_{0.5}Ta_{0.5})_{0.4}O_3$ thin films were fabricated and these showed a relaxor multiferroic property [23]. $Al_{0.5}Ga_{0.5}FeO_3$ has been shown to be multiferroic because of a non centrosymmetric space group characteristic of the crystal [24]. $La_2Ti_2O_7$ nanocrystals have been grown by a sol–gel method. These exhibit both ferroelectric and ferromagnetic behavior at room temperature. Also the material shows a rather large magnetodielectric effect, the magnetodielectric parameter having a value of 39.3% at 1 kHz under a magnetic field of 6 kOe [25].

Double perovskite oxides have received a lot of attention in recent years as part of search for multiferroic materials [26–36]. Though the emphasis has been on Bi-based perovskite compounds, lately rare-earth based oxides have also been investigated [33,11]. From the theoretical analyses of Bi-based compounds it has been predicted that a combination of d^5 and d^8 ions on the B sites of a perovskite lattice (ABO_3) would give the best results for obtaining a net spontaneous magnetization. In order to have a ferroelectric behavior simultaneously the presence of a cation having lone-pair s electrons is necessary to stabilize a noncentrosymmetric crys-

* Corresponding author. Tel.: +91 3324734971; fax: +91 3324732805.
E-mail address: mlsdc@iacs.res.in (D. Chakravorty).

0925-8388/$ – see front matter © 2011 Elsevier B.V. All rights reserved.
doi:10.1016/j.jallcom.2011.03.007

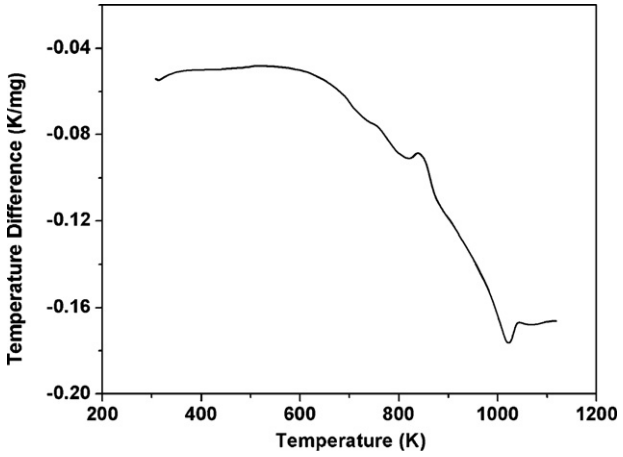

Fig. 1. DTA curve obtained from glass sample with composition 2 TeO_2·NiO·MnO (molar ratio).

tal structure [35]. Therefore we have explored the possibility of synthesizing Te_2NiMnO_6 crystals which satisfy the above requirements. Our approach has been to grow nanocrystals of the above phase within a glass medium. The composite indeed exhibits both ferroelectric and ferromagnetic orders. The details are reported in this paper.

2. Experimental details

The composition of the glass was $2TeO_2$·NiO·MnO (molar ratio). The precursor oxides used were AR grade. The oxides in appropriate amounts were mixed thoroughly with acetone. The powder was taken in an alumina crucible and melted in an electrically heated furnace at 1273 K. The melt was poured on an aluminium plate. The resultant glass was subjected to a Differential Thermal Analysis (DTA) by SDT Q600TA Instruments to determine the crystallization temperature [37]. Fig. 1 shows the DTA curve from which the required temperature was found to be 828 K. The glass sample was subjected to a heat-treatment at 828 K for 2 h to grow the crystalline phase. X-ray diffraction studies on the glass–crystal composite were carried out by a Bruker XRD SWAX using CuKα radiation. The microstructure was investigated by a JEOL 2010 Transmission Electron microscope operating at 200 kV. Magnetization measurements were carried out in the temperature range 2–300 K using a Quantum Design MPMS system with a SQUID Magnetometer. For dielectric measurements the glass-ceramic powders were compacted by a pressure of 5 tons/cm^2 using a mould with a diameter of 1 cm. Silver paint (supplied by Acheson Colloiden B.V., Netherlands) electrodes were applied on the two opposite faces of the pellets prepared as above. The Polarization-Electric field hysteresis was studied by a *P–E* loop tracer supplied by Marine India Pvt. Ltd. For magnetodielectric studies the pellets were inserted between the pole pieces of an electromagnet supplied by M/S Control Systems and Devices, Mumbai. Dielectric properties were measured for different values of magnetic field at room temperature using an Agilent-E4890A Impedance Analyzer

3. Results and discussion

Fig. 2 shows the X-ray diffraction pattern of the glass–crystal composite. The powder pattern was indexed by using the TREOR [38] computer programme. The intensities of the XRD patterns were extracted using the programme FULLPROF.2k (J. Rodriguez-Carvajal, FULLPROF.2k, Rietveld, Profile Matching and Integrated Intensity Refinement of X-ray and Neutron Data, Laboratoire Léon Brillouin, CEA, Saclay, France, 2001.) in the profile matching mode (without structure model). Pseudo-Voigt functions were used to fit the observed diffraction lines. The theoretical data are shown in Fig. 2. All the intensity peaks could be fitted as seen in this figure. The difference between experimental and theoretical intensities is also shown. The d_{hkl} and hkl values for all the peaks (indicated by serial numbers) are given in Table 1. The latter also shows the experimentally observed d_{hkl} and the corresponding FWHM values used for calculating particle diameters applying the Scherrer's formula [39]. The goodness of fit parameter is shown under this table. The values of lattice parameters extracted from the fitting of X-ray data are as follows: a = 1.03 nm, b = 0.797 nm, c = 0.724 nm,

Table 1
Comparison of interplanar spacing values obtained experimentally with those calculated by TREOR fitting.

X-ray diff. peak no.	X-ray diffraction d_{hkl} (nm)		hkl	FWHM (Exp.)	Particle diameter (nm)
	Experimental	Extracted by TREOR			
1	0.398	0.398	1 2 1	0.384	20.8
2	0.375	0.377	−2 1 2	0.295	27.2
3	0.366	0.366	1 1 2	0.295	27.2
4	0.353	0.352	3 0 1	0.246	32.7
5	0.326	0.326	−3 1 2	0.392	20.6
6	0.320	0.320	−3 2 1	0.217	37.2
7	0.309	0.306	1 2 2	0.240	33.0
8	0.296	0.296	2 3 0	0.435	18.7
9	0.280	0.280	4 0 1	0.282	29.0
10	0.273	0.272	2 3 1	0.284	28.8
11	0.266	0.265	1 1 3	0.246	33.4
12	0.261	0.262	3 3 0	0.147	55.7
13	0.256	0.256	0 2 3	0.295	27.9
14	0.242	0.242	3 3 1	0.196	42.1
15	0.230	0.230	5 0 1	0.492	17.0
16	0.219	0.219	−1 4 2	0.596	14.1
17	0.206	0.206	6 1 0	0.393	21.5
18	0.202	0.202	5 3 0	0.295	28.8
19	0.193	0.193	4 1 3	0.295	29.0
20	0.186	0.186	4 4 1	0.246	35.1
21	0.180	0.180	−3 5 1	0.286	30.3
22	0.178	0.178	3 1 4	0.286	30.4
23	0.174	0.174	−4 4 3	0.286	30.6
24	0.171	0.171	−4 0 5	0.246	35.8
25	0.164	0.164	0 6 1	0.492	18.1
26	0.160	0.160	−6 4 2	0.347	25.8
27	0.155	0.155	3 6 0	0.288	31.2
28	0.151	0.151	1 0 5	0.393	23.3
29	0.148	0.147	1 7 0	0.395	23.3
30	0.141	0.143	4 7 2	0.395	23.7

R factors: R_w = 21.9, R_{wp} = 21.2, R_{exp} = 14.1, GoF = (R_w/R_{exp}) = 1.55.

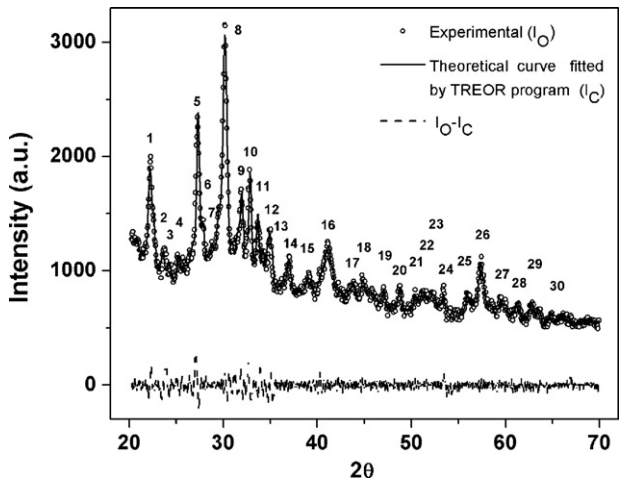

Fig. 2. X-ray diffractogram obtained from glass specimen containing Te_2NiMnO_6 crystal and the theoretical fitting of data by TREOR program.

$\alpha = 90^\circ$, $\beta = 102.4^\circ$, $\gamma = 90^\circ$. Evidently, the nanocrystals grown have a monoclinic symmetry.

Fig. 3(a) is a transmission electron micrograph for the composite system. It can be seen that there are crystals having diameters in the range 17–41 nm. There are also some large crystals with dimensions around 333 nm. We have estimated the crystallite sizes from the line broadening of the X-ray diffraction peaks by using Scherrer's formula [39]. The latter gives a crystallite size range 18–55 nm. This is in satisfactory agreement with TEM results. In Fig. 3(b) is the electron diffraction pattern obtained from the large crystal as shown in the inset. It is evident that the particle consists of a single crystal. The interplanar spacings calculated from the diffraction spots are summarized in Table 2. They are compared with the values extracted from the X-ray diffraction data. The two of them are in satisfactory agreement.

Fig. 4 shows the variation of magnetization as a function of temperature under both zero field-cooled (ZFC) and field-cooled (FC) conditions. Both curves show a continuous increase in magnetization as the temperature is lowered. They also exhibit a hump at around 32 K. The latter is believed to arise due to an antiferromagnetic super exchange interaction between the spins of Ni^{2+} and Mn^{2+} ions respectively and corresponds to the Neel temperature of this system. The continuous rise in the magnetization value even in the ZFC case signifies a one-dimensional configuration of these ions and a consequent Heisenberg antiferromagnetic model being operative here [40]. This therefore implies that the Te_2NiMnO_6 nanocrystals form a percolative network and the spins at the surfaces of these form the one-dimensional configuration.

Table 2
Comparison of interplanar spacing values calculated from electron diffraction pattern with those extracted from X-ray diffraction analysis using TREOR computer programme.

Electron diffraction d_{hkl} (nm)	X-ray diffraction d_{hkl} (nm) (extracted by TREOR)	hkl
0.298	0.296	230
0.265	0.265	113
0.230	0.230	510
0.207	0.206	610
0.195	0.193	413
0.177	0.178	314
0.171	0.171	−405
0.160	0.160	−642
0.152	0.151	105
0.147	0.147	170

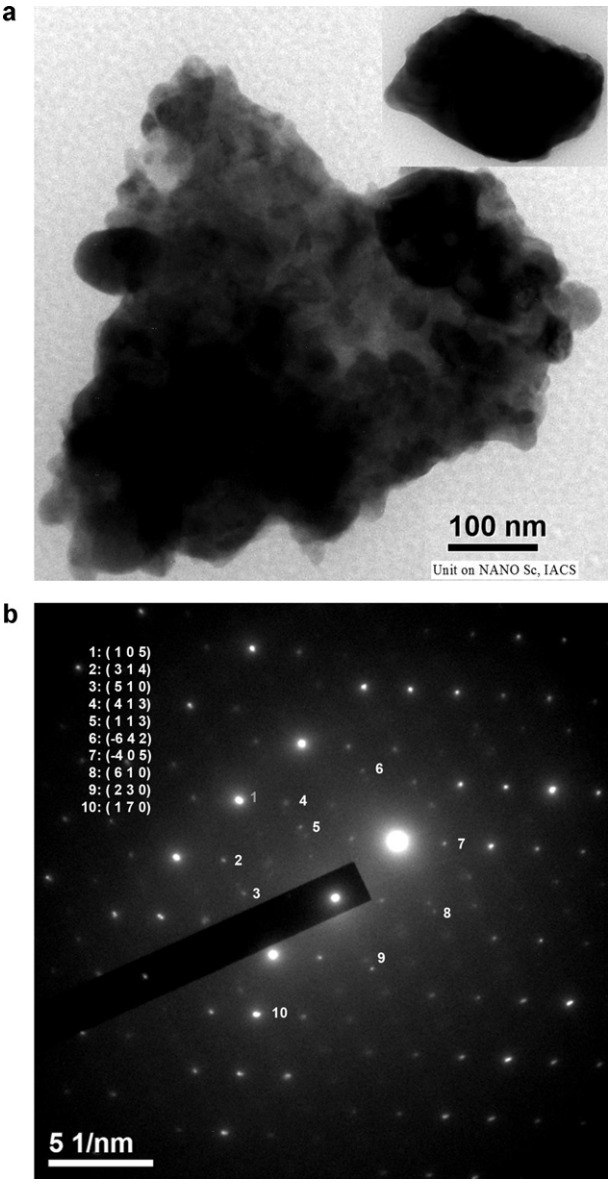

Fig. 3. (a) Transmission electron micrograph of nanocomposite sample (b) Electron diffraction pattern obtained from fig. 3(a) inset.

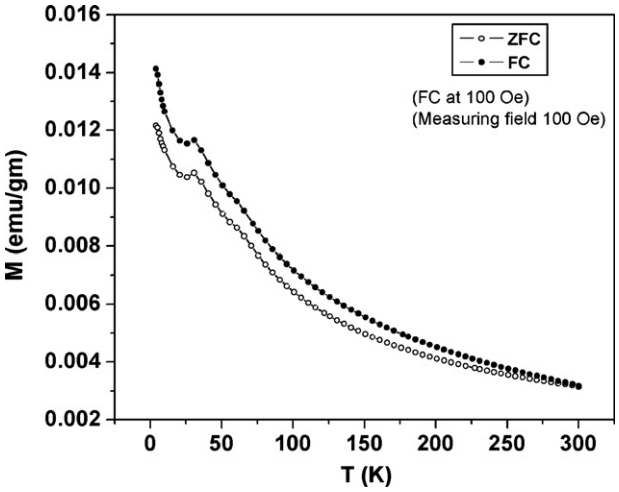

Fig. 4. Variation of magnetization as a function of temperature under Zero field-cooled (ZFC) and field-cooled (FC) conditions for nanocomposite containing Te_2NiMnO_6.

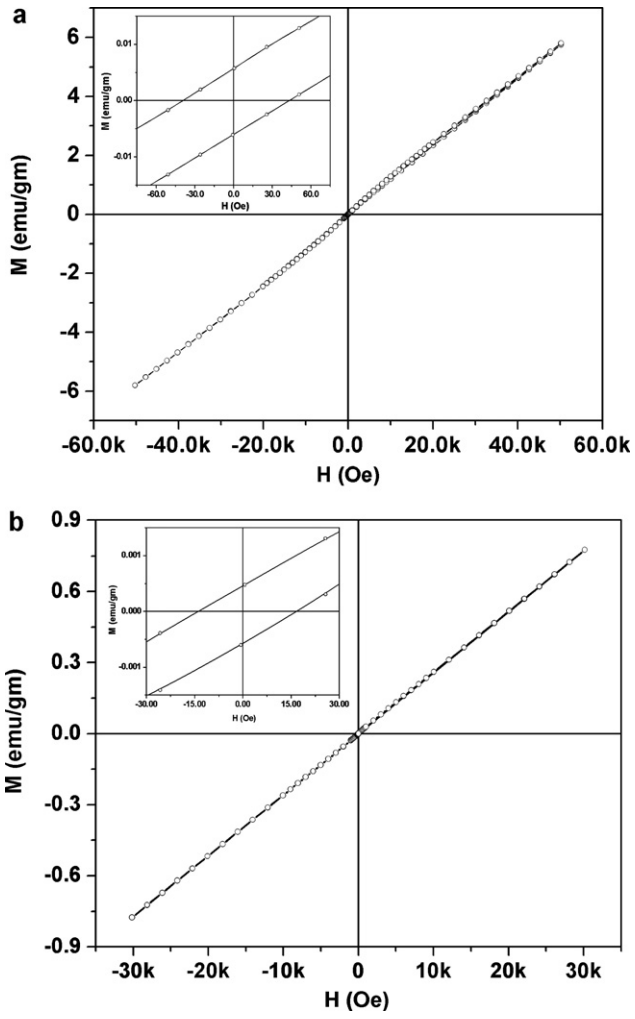

Fig. 5. Magnetization vs. magnetic field hysteresis loops for Te_2NiMnO_6 containing nanocomposite at different temperatures. (a) 5 K (b) 300 K.

The nanocomposites exhibit a weak ferromagnetic behavior at temperatures in the range 2–300 K. Fig. 5(a) and (b) shows the magnetization vs. magnetic field curves for temperatures 5 K and 300 K respectively. The expanded views are shown in the insets of these figures. These are typical of the results obtained at other temperatures. The coercivity was found to increase as the temperature was lowered. Table 3 summarizes the results. This is consistent with the equation relating H_c to temperature for magnetic nanoparticles [41] viz.,

$$H_c = H_{c_0}\left[1 - \left(\frac{T}{T_B}\right)^{\frac{1}{2}}\right] \quad (1)$$

where H_c is the coercivity, H_{c_0} is a constant, T is the temperature and T_B is the blocking temperature for a superparamagnetic particle.

In Fig. 6 is shown the Dielectric Polarization vs. Electric Field curve. A hysteresis is obtained signifying a ferroelectric behavior. It is to be noted that the dissipation factor ($\tan\delta$) measured

Table 3
Coercivity values of nanocomposites at different temperatures.

Temperature (K)	Coercivity (Oe)
5	38.7
10	22.2
20	19.3
30	16.7
300	13.8

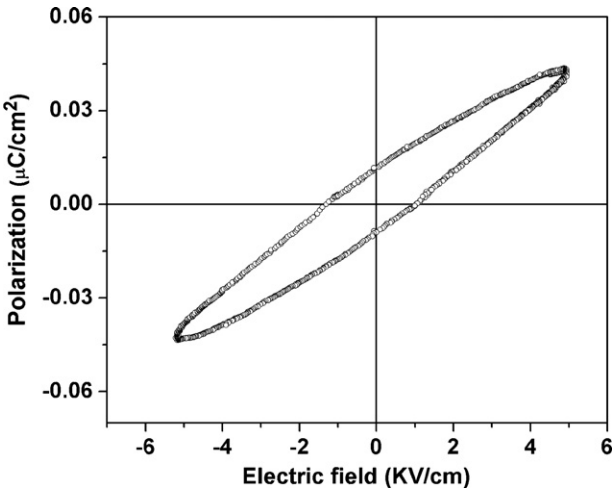

Fig. 6. Polarization–Electric field hysteresis loop for nanocomposite sample at room temperature.

at 50 Hz for the sample is found to be 0.015. The leakage current at 1 V is 2.5×10^{-10} A.The remanent polarization is found to be 0.015 μC/cm^2. This value is small. Using the concept of tolerance factor (t) defined as $t = (r_A + r_O)/\sqrt{2}(\overline{r_B} + r_O)$ where r_O and r_A are the ionic radii of the O, and A ions respectively and $\overline{r_B}$ is the average ionic radius of the B site cations in the double perovskite structure [42–44], we have calculated a value of $t = 0.805$ for our system. A value of $t < 1$ has been shown to introduce a lattice instability (so-called *A*-site driven) causing off-centering of the *A*-site ions and BO_6 octahedral tilts. On the basis of this analysis, it is also expected that our specimen system should exhibit the ferroelectric behavior. Fig. 7(a) shows the variation of dielectric constant as a function of the applied magnetic field. The dielectric constant increases up to a magnetic field of 10 kGauss. The magnetodielectric parameter (MD) defined as $\frac{\varepsilon(H)-\varepsilon(0)}{\varepsilon(0)} \times 100$ is estimated to be 0.55% where $\varepsilon(H)$ and $\varepsilon(0)$ are the values of dielectric constant at magnetic field H and zero respectively. This value is larger than those reported in recent years for other multiferroic systems like Bi_2NiMnO_6 [45], $BiFeO_3$ [46], and $BaTiO_3$–$LaMnO_3$ composites [47]. The values in the latter have been found to be in the range 0.03–0.1%. In Fig. 7(b) is shown the variation of dissipation factor ($\tan\delta$) as a function of the magnetic field applied. It is seen that the dissipation factor shows a decreasing trend as the magnetic field is increased. The MD effect is ascribed to

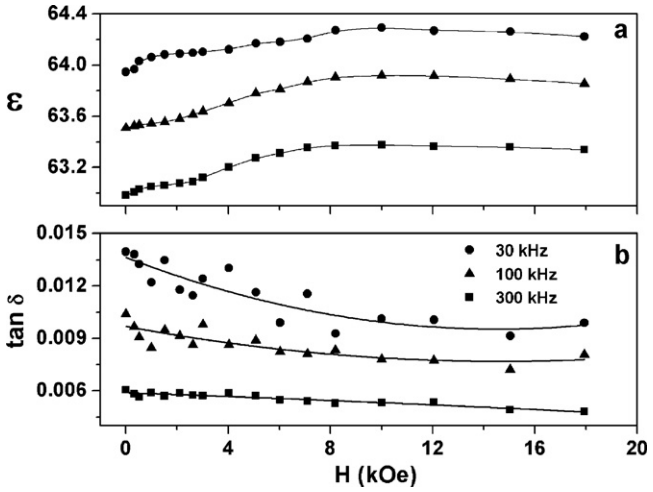

Fig. 7. (a) Variation of dielectric constant as a function of magnetic field at room temperature for the nanocomposite. (b) Variation of dissipation factor as a function of magnetic field at room temperature for the nanocomposite.

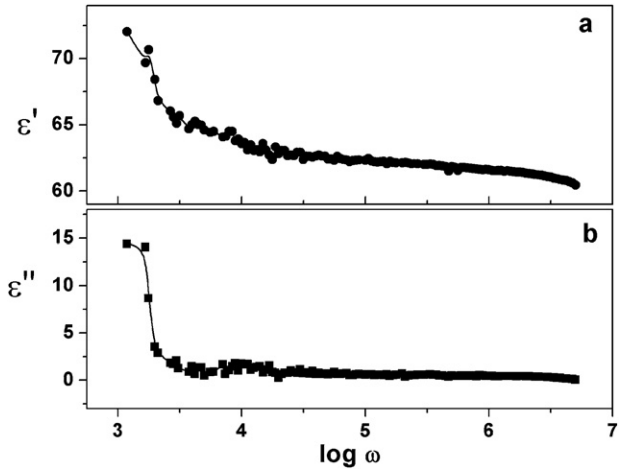

Fig. 8. (a) Variation of real part ε' of dielectric permittivity as a function of log (angular frequency). (b) Variation of imaginary part ε" of dielectric permittivity as a function of log (angular frequency).

the effect of magnetostriction in Te_2NiMnO_6 phase which increases the crystal asymmetry thereby increasing the value of the permanent dipole moment of the crystal. This brings about an increase in the value of the dielectric constant. It is to be noted that the dielectric constant value increases as the measurement frequency is decreased. This is a characteristic feature for a dielectric material having a relaxation mechanism operating in it. In order to substantiate this conclusion we have shown in Fig. 8(a) and (b) the variation of real part ε' and imaginary part ε" of the dielectric permittivity as a function of log ω (ω being the angular frequency of the applied ac voltage) respectively. It can be seen that there is a maximum in ε" corresponding to the frequency at which ε' has a point of inflection. This has been ascribed to a Debye-like relaxation [48].

The present investigation and the results obtained in it could be of interest for applied research. Magnetic field sensors of nanoscale dimensions could be fabricated using the materials synthesized in this study.

4. Conclusions

Nanocrystals of Te_2NiMnO_6 perovskite oxide with dimensions in the range 17–41 nm were grown within a glass matrix formed by melting a precursor mix of $2TeO_2{\cdot}NiO{\cdot}MnO$ (molar ratio). The lattice parameters were determined from the X-ray diffraction data by using the TREOR computer programme. The crystal symmetry was found to be monoclinic. The samples showed a weak ferromagnetic behavior over the temperature range 2–300 K. They also exhibited a ferroelectric hysteresis at room temperature with a remanent polarization of 0.015 $\mu C/cm^2$. The specimens showed a magnetodielectric behavior with the dielectric constant increasing as a function of the applied magnetic field. The MD parameter obtained by the present system was 0.55%. The present approach will open up possibilities of synthesizing new perovskite oxides with multiferroic behavior.

Acknowledgment

The research was supported by Nano Mission of the Department of Science and Technology, Govt. of India, New Delhi. R.P. Maiti thanks Council of Scientific and Industrial Research, Govt. of India, New Delhi for the award of a Senior Research Fellowship. D.Chakravorty thanks the Indian National Science Academy, New Delhi for awarding an honorary scientist's position. Support for this work was also derived from a grant of Department of Science and Technology, New Delhi under an Indo-Australian project on Nanocomposite Materials for Clean Energy.

References

[1] Y.J. Wu, L.H. Tang, H.L. Li, X.M. Chen, J. Alloys Compd. 496 (2010) 269.
[2] C.F. Yao, Z.Q. Lia, J.K. Shang, J. Alloys Compd. 502 (2010) 492.
[3] L. Zhu, Y. Dong, X. Zhang, Y. Yao, W. Weng, G. Han, N. Ma, P. Du, J. Alloys Compd 503 (2010) 426.
[4] Felicia Prihor Gheorghiu, Adelina Ianculescu, Petronel Postolache, Nicoleta Lupu, Marius Dobromir, Dumitru Luca, Liliana Mitoseriu, J. Alloys Compd. 506 (2010) 862.
[5] R. Rai, A.L. Kholkin, S. Sharma, J. Alloys Compd. 506 (2010) 815.
[6] G. Alvarez, H. Montiel, J.A. Peña, M.A. Castellanos, R. Zamorano, J. Alloys Compd. 508 (2010) 471.
[7] X. Zheng, Q. Xu, Z. Wen, X. Lang, D. Wu, T. Qiu, M.X. Xu, J. Alloys Compd. 499 (2010) 108.
[8] N. Kumar, N. Panwar, B. Gahtori, N. Singh, H. Kishan, V.P.S. Awana, J. Alloys Compd. 501 (2010) L29.
[9] Adelina Ianculescu, Felicia Prihor Gheorghiu, Petronel Postolache, Ovidiu Oprea, Liliana Mitoseriu, J. Alloys Compd. 504 (2010) 420.
[10] N.V. Minh, D.V. Thang, J. Alloys Compd. 505 (2010) 619.
[11] S. Chen, L. Wang, H. Xuan, Y. Zheng, D. Wang, J. Wu, Y. Du, Z. Huang, J. Alloys Compd. 506 (2010) 537.
[12] X. Zhang, Y. Sui, X. Wang, Y. Wang, Z. Wang, J. Alloys Compd. 507 (2010) 157.
[13] P. Thakuria, P.A. Joy, Appl. Phys. Lett. 97 (2010) 162504.
[14] Y.H. Gu, Y. Wang, F. Chen, H.L.W. Chan, W.P. Chen, Y.H. Gu, J. Appl. Phys. 108 (2010) 094112.
[15] S. Farhadi, N. Rashidi, J. Alloys Compd. 503 (2010) 439.
[16] Z. Dai, Y. Akishige, J. Phys. D: Appl. Phys. 43 (2010) 162504.
[17] J. Wu, S. Mao, Z.-G. Ye, Z. Xie, L. Zheng, J. Mater. Chem. 20 (2010) 6512.
[18] X. Zhu, Y. Yang, K. He, J. Zhu, S. Ye, S. Zhou, Z. Liu, Ferroelectrics 409 (2010) 204.
[19] J. Wu, J. Wang, J. Alloys Compd. 507 (2010) L4.
[20] J. Wu, J. Wang, J. Appl. Phys. 108 (2010) 026101.
[21] S. Cui, J. Alloys Compd. 508 (2010) 520.
[22] C.S. Park, Y.-S. Shin, J.Y. Son, Y. Shon, T.W. Kang, Y.D. Park, Solid State Commun. 150 (2010) 2131.
[23] A. Dilsom, A. Sanchez, N. Kumar, R. Ortega, S. Katiyar, J.F. Scott, Appl. Phys. Lett. 97 (2010) 202910.
[24] A. Shireen, R. Saha, P. Mandal, A. Sundaresan, C.N.R. Rao, J. Mater. Chem. 21 (2011) 57.
[25] L. Sun, J. Hu, F. Gao, X. Kong, H. Qin, M. Jiang, J. Alloys Compd. 502 (2010) 176.
[26] Y. Du, Z.X. Cheng, S.X. Dou, X.L. Wang, H.Y. Zhao, H. Kimura, Appl. Phys. Lett. 97 (2010) 122502.
[27] S.A. Ivanov, P. Nordblad, R. Mathieu, R. Tellgren, C. Ritter, Dalton Trans. 39 (2010) 11136.
[28] E. Langenberg, J. Rebled, S. Estradé, C.J.M. Daumont, J. Ventura, L.E. Coy, M.C. Polo, M.V. García-Cuenca, C. Ferrater, B. Noheda, F. Peiró, M. Varela, J. Fontcuberta, J. Appl. Phys. 108 (2010) 123907.
[29] D. Choudhury, A. Hazarika, A. Venimadhav, C. Kakarla, K.T. Delaney, P.S. Devi, P. Mondal, R. Nirmala, J. Gopalakrishnan, N.A. Spaldin, U.V. Waghmare, D.D. Sarma, Phys. Rev. B 82 (2010) 134203.
[30] I. Alvarez-Serrano, I. Ruiz de Larramendi, M.L. López, C. Pico, T. Rojo, M.L. Veiga, J. Alloys Compd. 509 (2011) 1457.
[31] M. Lezaic, N.A. Spaldin, Phys. Rev. B 83 (2011) 024410.
[32] M. Azuma, K. Takata, T. Saito, S. Ishiwata, Y. Shimakawa, M. Takano, J. Am. Chem. Soc. 127 (2005) 8889.
[33] R.J. Booth, R. Fillman, H. Whitakener, A. Nag, R.M. Tiwan, K.V. Ramanujachary, J. Gopalakrishnan, S.E. Lofland, Mater. Res. Bull. 44 (2009) 1559.
[34] L. Ortega-San Martin, J.P. Chapman, G. Cuello, J. Gonzalez-Calbet, M.I. Arriortua, T. Rojo Aparicio, Z. Anorg, Allg. Chem. 631 (2005) 2127.
[35] P. Baettig, C. Ederer, N.A. Spaldin, Phys. Rev. B 72 (2005) 214105.
[36] T. Wang, W. Xu, X. Fang, W. Dong, R. Tao, D. Li, Y. Zhao, X. Zhu, J. Alloys Compd. 475 (2009) 9.
[37] R.P. Maiti, S. Basu, S. Bhattacharya, D. Chakravorty, J. Non-Cryst. Solids 355 (2009) 2254.
[38] P.E. Werner, TREOR, A Trial and Error Programme for Indexing Unknown Powder Patterns, University of Stockholm, Sweden, 1984.
[39] B.D. Cullity, S.R. Stock, Elements of X-ray diffraction, 3rd ed., Prentice-Hall, Upper Saddle River, NJ, USA, 2001.
[40] M. Steiner, J. Villain, C.G. Windsor, Adv. Phys. 25 (1976) 87.
[41] J.R. Childress, C.L. Chien, M. Nathan, Appl. Phys. Lett. 56 (1) (1990) 95.
[42] R.D. Shannon, Acta Crystallogr. Sect. A 32 (1976) 751.
[43] D.J. Singh, C.H. Park, Phys. Rev. Lett. 100 (2008) 087601.
[44] A. Faik, E. Iturbe-Zabalo, I. Urcelay, J.M. Igartua, J. Solid State Chem. 182 (2009) 2656.
[45] P. Padhan, P. LeClair, A. Gupta, G. Srinivasan, J. Phys. Condens. Matter. 20 (2008) 355003.
[46] Y.-K. Jun, W.-T. Moon, C.-M. Chang, H.-S. Kim, H.S. Ryu, J.W. Kim, K.H. Kim, S.-H. Hong, Solid State Commun. 135 (2005) 133.
[47] N.G. Kim, Y.S. Koo, C.J. Won, N. Hur, J.H. Jung, J. Yoon, Y. Jo, M.H. Jung, J. Appl. Phys. 102 (2007) 014107.
[48] C. Kittel, Introduction to Solid State Physics, John Wiley & Sons, New York, London, 1961, p.176.